RSC Advances

PAPER

View Article Online
View Journal | View Issue

Cite this: *RSC Adv.*, 2015, **5**, 26521

Chemically anchored NiO_x–carbon composite fibers for Li-ion batteries with long cycle-life and enhanced capacity

Yanli Gong,[ab] Ming Zhang*[a] and Guozhong Cao*[cd]

N-doped carbon fibers and their composites have drawn much attention because of their wide application in energy storage. In this paper, NiO_x nanoparticles are anchored on N-doped carbon fibers by chemical bonds with controlled concentration of NiO_x, and the fibers interweave into hierarchical structured networks. It is demonstrated that these NiO_x nanoparticles consisted of both NiO and Ni^0 other than a single phase. As binder-free anodes for lithium-ion batteries, the NiO_x–C fiber networks obtained at 650 °C with 9.2 wt% NiO_x could deliver a specific capacity of 676 mA h g^{-1} after 200 cycles at a current density of 500 mA g^{-1}. It is also found that the storage and rate capacities of the networks are dependent on both the content of NiO_x and the annealing temperature. The improved lithium-ion storage properties can be ascribed to the intimate connection between NiO_x and the highly conductive network of carbon fibers through chemical bonds.

Received 26th January 2015
Accepted 6th March 2015

DOI: 10.1039/c5ra01518a

www.rsc.org/advances

1 Introduction

In spite of successful commercialization of lithium-ion batteries (LIBs) for more than two decades, intense research efforts have been devoted to develop new electrode materials for LIBs to meet the ever increasing demand for high energy and power density as well as good cyclic stability for energy and power hungry of new generation electronics and electric vehicles.[1–3] Compared to commercial graphitic anodes with a theoretical capacity of 372 mA h g^{-1}, transition metal oxides (TMOs) have attracted much attention because of their higher theoretical capacities, for example 717 mA h g^{-1} for NiO,[4,5] 674 mA h g^{-1} for CuO,[6] and 924 mA h g^{-1} for Fe_3O_4.[7] As their lithium ion storage mechanism is based on conversion reactions, TMOs always suffer from the issue of electrode pulverization arising from the huge volumetric change during lithiation/delithiation processes.[8] Among the TMOs mentioned above, NiO with low cost and relatively high theoretical capacity has been investigated by many researchers.[9–13] A variety of strategies have been developed to improve the properties of NiO as anodes for LIBs, such as preparing nanosized and/or hollow structured NiO,[4] and modifying them with carbon materials.[11,12] Since carbon materials with high electrical conductivity and excellent stability for LIBs are commercial anodes, a lot of researches have been focused on the preparation of NiO–carbon composites with various architectures in nano-, meso- and microscales, which were the research hot-pot of NiO based anodes for LIBs.

Amorphous carbon, carbon nanotubes, graphene, and carbon fibers were commonly employed to modify NiO to improve their conductive and stability properties.[14,15] For example, both spherical and net-structured NiO were modified with carbon by a hydrothermal method to achieve enhanced properties.[16,17] Carbon nanotubes were also used to prepare NiO–carbon composites *via* a surface modifying method.[18] However, NiO in those composites were not intimately mixed and well protected by carbon materials because they were not coated by carbon. Graphene, a new kind of carbon materials with excellent electrical and mechanical properties, was used to modify NiO and other TMOs.[7,11,12,19–21] Synthesis of NiO–graphene commonly began with nickel salts and graphene oxide, and the resultant NiO–graphene composites were easily to stack up to block the diffusion of lithium ions, resulting in a low capacity at a large current density. In comparison, composites based on carbon fiber can protect TMOs from pulverization and improve the fast transfer of electron owing to carbon fiber networks and easily diffusion of lithium ions because of large interface between electrolyte and active materials.[22–26] Preparing properly designed NiO–carbon fiber nanocomposites may be a strategy to enhance their properties.

Ni (or NiO)–carbon fiber composites have attracted much interest in the fields of LIBs,[27–32] supercapacitors,[33] and catalysts.[34] Those composites commonly fabricated by means of

[a]*Key Laboratory for Micro-Nano Optoelectronic Devices of Ministry of Education, School of Physics and Microelectronics, State Key Laboratory for Chemo/Biosensing and Chemometrics, Hunan University, Changsha, 410082, China. E-mail: zhangming@hnu.edu.cn*

[b]*College of Automotive Engineering, Hunan Industry Polytechnic, Changsha, 410208, China*

[c]*Department of Materials Science & Engineering, University of Washington, Seattle, Washington, 98195, USA. E-mail: gzcao@uw.edu*

[d]*Beijing Institute of Nanoenergy and Nanosystems, Chinese Academy of Sciences, Beijing 100083, China*

electrospinning using polyacrylonitrile and nickel salts as precursors, and followed with annealing/pyrolysis treatment in an inert gas at high temperatures.[27–29] It should be noted that the standard electrode potential of Ni^{2+}/Ni ($\varphi_A^{\ominus} = -0.257$ V) is higher than that of Co^{2+}/Co ($\varphi_A^{\ominus} = -0.277$ V), Ni^{2+} would be reduced by carbon (or CO) more easily than that of Co^{2+}.[35] Cobalt compounds in electrospun CoO_x–C fibers have been reported to be Co^0.[36] Similarly, most of the final product of Ni(or NiO)–carbon fiber composites were Ni–carbon fiber composites.[27–29] Considering the fact that TMOs storing lithium ions is based on the conversion reaction, transition metal do not have direct contribution on the storage of lithium ions.[37] However, some Ni–carbon fiber composites have been reported to show improved specific capacity as compared to pure carbon fibers.[27] Similar results were found in Co–carbon fiber composites as advanced anodes for LIBs.[36] Therefore, it is of great significance to figure out the valence of nickel and the mechanism of NiO_x improving the properties of carbon fibers.

In this study, NiO_x–carbon fiber nanocomposites were synthesized by electrospinning starting from polyacrylonitrile and nickel acetate tetrahydrate ($NiAc_2$). After heat treated in N_2 at a high temperature (about 650 °C), polyacrylonitrile was pyrolyzed to carbon, and $NiAc_2$ was converted to nickel oxide and partially to nickel (Ni^0), which was confirmed by means of XPS analysis. The composites showed improved excellent cyclic stability and specific capacities especially at large current densities. The improvement may be ascribed to the carbon fiber networks with high conductivity and fast diffusion rate of lithium ions, the present of nickel nanoparticles in the composites, and the chemical bonds between nickel and carbon.

2 Experimental sections

Polyacrylonitrile (PAN, $M_w = 150\,000$, Sigma-Aldrich Co., Ltd., USA), $NiAc_2$ (Alfa Aesar Co., Ltd., USA), and *N*,*N*-dimethylformamide (DMF, J. T. Baker Co., Ltd. USA) were purchased from the companies and used without any purification. To prepare the precursor for electrospinning, PAN and $NiAc_2$ were dissolved in DMF to form solutions with concentrations of 6.5 wt% and 1.6–2.3 wt%. Then they were transferred to a 3 mL syringes with a stainless steel needle whose inner diameter was 0.6 mm. The flow rate of the precursor solution was set to about 0.4 mL h^{-1} by a syringe pump. A piece of aluminum foil, which was vertically positioned about 15 cm away from the needle, was used as the collector for fibers. The potential between the needle and the collector was controlled to be 13–17 kV by a high voltage DC power. Finally, a piece of PAN–$NiAc_2$ fiber network was obtained from the aluminum foil. After being treated in air at 225 °C for 6 h, the resulting brown networks were annealed at 550–700 °C in N_2 for 2 h to carbonize the PAN and decompose the $NiAc_2$. When the weight ratio of $NiAc_2$ in precursor solutions was 1.95%, the final products obtained at different temperature were A-2-X (X means the final annealed temperature). When $NiAc_2$ was 1.6 wt% and 2.3 wt% in precursor solutions, the final products were marked as B-2-X and C-2-X, respectively. Pure carbon fibers were synthesized using PAN solution without any $NiAc_2$. Carbon fibers synthesized at 650 °C were marked as E650.

The microstructure and morphology of composites were characterized using a JEOL JSM-7000F scanning electron microscope (SEM), and a FEI Tecnai G2 F20 transmission electron microscope (TEM) operating at 200 kV accelerating voltage. Elemental analysis of samples was achieved using energy dispersive spectroscopy (EDS) on SEM. Thermogravimetric analysis (TGA) data were collected on a Netzsch STA449C thermal analyzer. The valence of the atoms in samples was detected by X-ray photoelectron spectroscopy (XPS, Surface Science Instruments S-probe spectrometer).

The binding energy scale was calibrated by assigning the lowest binding energy of the C 1s peak to a binding energy of 285.0 eV.

Fiber networks (including NiO_x–C, carbon fibers) were directly used as binder-free anodes for LIBs. A Celgard 2400 microporous polypropylene membrane was used as a separator. A solution of 1 M $LiPF_6$ in ethylene carbonate–dimethyl carbonate (1 : 1 by volume) was used as electrolyte to assemble coin cells (CR-2016). Pure lithium foils were used as both counter and reference electrodes. All of the coin-cells were assembled in an argon-filled glove-box with the moisture and oxygen levels less than 1 ppm. Discharge and charge measurements were carried out using Arbin BT2000 and LAND battery testing systems with the cut off potentials being 0.005 V for discharge and 3 V for charge. The cyclic voltammetry curves were collected on an electrochemical workstation (CHI660B).

3 Results and discussion

Fig. 1 displays the SEM images of pure carbon fibers, and NiO_x–C fibers with different weight ratios of NiO_x. Fig. 1a shows pure carbon fibers (E650) exhibiting smooth surface, with uniform diameters of about 200 nm and length for several micrometers. Fig. 1b confirms the NiO_x–C fibers (B-2-650) with very few nanoparticles when the weight ratio of $NiAc_2$ in the precursor solution was 1.6 wt%. As the $NiAc_2$ weight ratio in precursor increased to 2.3 wt%, NiO_x–C fibers (C-2-650) with inhomogeneous distribution of nanoparticles are observed in Fig. 1c. If the $NiAc_2$ concentration was adapted to be a suitable level of 1.95 wt%, the resulted fibers (A-2-650) with homogenous distribution of nanoparticles in a local field could be achieved, as shown in Fig. 1d. Fig. 1e is a low-resolution SEM image of the sample A-2-650, showing those fibers with uniform diameters and lengths more than 20 μm forming a network. This phenomenon is similar to our previous study about CoO–carbon fiber mats,[23] indicating that the framework of carbon fibers are not changed by neither CoO nor NiO_x. The A-2-650 sample was characterized by EDS further. The EDS results shown in Fig. 1f reveal the presence of Ni, C, O, and N, while the N is the residual nitrogen from PAN.[23]

Fig. 2 compares the TGA thermograms of NiO_x–C fiber samples. There is little weight loss at the temperature below 300 °C which could be attributed to the desorption of adsorbed water. The sharp weight loss in B-2-650 (lowest concentration of NiO_x among three samples) is higher than those of both A-2-650

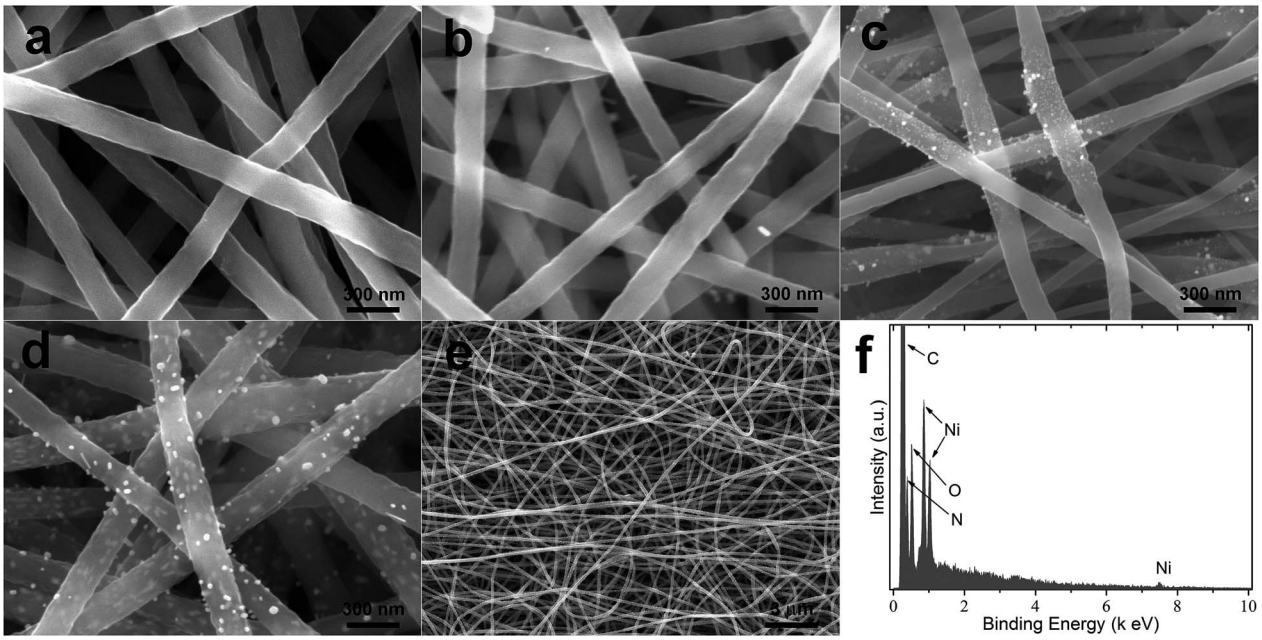

Fig. 1 SEM image of pure carbon fibers (E650, a) and NiO_x–C fibers (B-2-650, (b); C-2-650, (c); A-2-650, (d) and (e)), and the EDS spectrum of A-2-650 (f). All of those samples were obtained at 650 °C in Ar for 2 h.

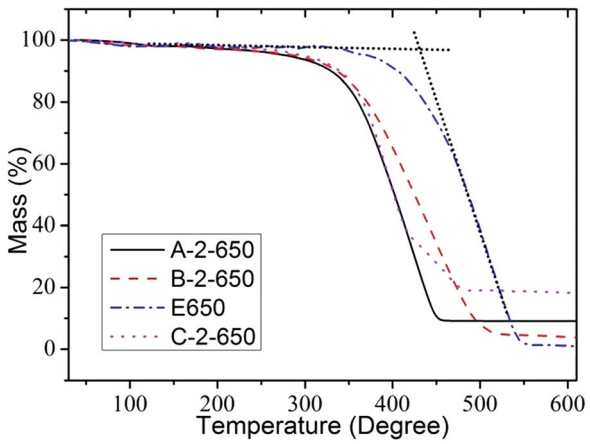

Fig. 2 TGA thermograms of NiO_x–C fibers with different nickel concentrations and pure carbon fibers (E650). The experiments were carried out at a heating rate of 5 °C min^{-1} in air with a flow rate of 20 mL min^{-1}.

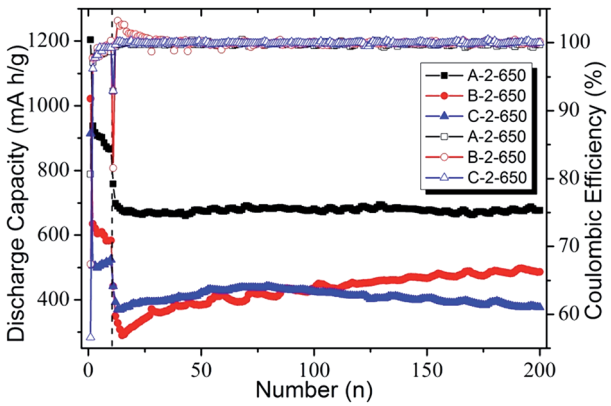

Fig. 3 The specific capacities, cyclic properties and Coulombic efficiencies of three NiO_x–C fibers at different current density: 100 mA g^{-1} in the range of 1 to 10 cycles and 500 mA g^{-1} in subsequent cycles.

and C-2-650, showing a negative effect of NiO_x on the thermal stability of NiO_x–C fibers. A possible reason is that Ni or NiO may be a catalyst for the oxidation of carbon.[27] When the temperature increased higher than 550 °C, the weight of those samples were changeless at 9.2%, 3.2%, and 17.1% for A-2-650, B-2-650, and C-2-650, showing good stability of the final products. According to the literature, they could be indexed to NiO.[28] Therefore, the NiO_x in the samples A-2-650, B-2-650, and C-2-650 could be roughly estimated to be 9.2 wt%, 3.2 wt%, and 17.1 wt%, respectively.

The electrochemical properties of above NiO_x–C fibers with regards to the storage of lithium ions were estimated by assembling and measuring coin cells, and the results are shown in Fig. 3. The initial discharge capacities of A-2-650, B-2-650, and C-2-650 are 1203, 1022, and 914 mA h g^{-1}, corresponding to Coulombic efficiencies of 80%, 67%, and 57%, respectively. Owing to the irreversible formation of solid electrolyte interphase (SEI) films in the first lithiation procedure, their discharge capacities decrease to 938, 635, and 506 mA h g^{-1} in the second cycle, respectively. After lithiation/delithiation processing at a current density of 100 mA g^{-1} for ten times, the discharge capacity of A-2-650 is as high as 865 mA h g^{-1} while they are only 582 and 524 mA h g^{-1} for B-2-650 and C-2-650, indicating that the weight ratio of NiO_x has great effect on the electrochemical properties of NiO_x–C fibers. After the current

density increases to 500 mA g^{-1} at the 11th cycle, the A-2-650 could deliver a discharge capacity of 676 mA h g^{-1}, which is 1.4 and 1.8 times that of B-2-650 and C-2-650. In addition, the Coulombic efficiency of A-2-650 is fixed at approximate 100% at a current density of 500 mA g^{-1}, showing a better cyclic stability of A-2-650 as compare to either B-2-650 or C-2-650. Therefore, the most suitable concentration of NiO_x in NiO_x–C fibers may be around 9.2 wt%, which is very close to a published paper about Ni/C composites as anodes for LIBs with highest capacity.[28] The fibers fabricated from the precursor solution with 1.9 wt% $NiAc_2$ were investigated in detail in subsequent research.

Fig. 4a shows a TEM image of A-2-650 at a low magnification. Uniform carbon fibers with some nanoparticles on their surface are clearly visible. In an amplified TEM image (Fig. 4b), lots of fine nanoparticles are found inside the carbon fibers. The nanoparticles attached on the surface of carbon fibers are relative larger than those inside the carbon fibers, indicating that carbon matrix can suppress the growth of nanoparticles. A high-resolution TEM image in Fig. 4c shows four small nanoparticles on the edge of the fiber and a large one outside the fiber. Fig. 4d shows an amplified image of the marked area in Fig. 4c. The regular lattice fringes with three spaces of 0.203, 0.176, and 0.208 nm are highly consistent with the *d* values of the (111) and (200) planes of Ni^0 (JCPDS 4-850), and the (200) plane of NiO (JCPDS 47-1049), suggesting that those nanoparticles are NiO and Ni^0. The high-resolution image of the large nanoparticle in Fig. 4c displays lattice fringes of 0.203 and 0.176 nm which could be ascribed to *d* values of the (111) and (200) planes of Ni^0 (JCPDS 4-850). These results reveal that most of nanoparticles on the surface of the fiber are Ni^0. Thus the microstructure of NiO_x–C fibers is schematically displayed in Fig. 4f that most of nanoparticles on the surface of carbon fibers are Ni^0 nanoparticles.

XPS analysis was conducted to determine the bond state of nickel in NiO_x–C fibers. The experiments were carried out on a Surface Science Instruments S-probe spectrometer, which had a monochromatized Al K_α X-ray source and a low energy electron flood gun for charge neutralization of nonconducting samples. The XPS spectrum of A-2-650 NiO_x–C fibers is shown in Fig. 5a, which reveals the present of carbon, nitrogen, oxygen, and nickel. This result is highly consistent with the conclusion of EDS that carbon fibers are doped by nitrogen. Fig. 5b shows the Ni 2p XPS spectrum of A-2-650, which can be deconvoluted to three peaks with a Gaussian fit. The main peak at 855.1 eV associated a satellite peak at 860.9 eV is attributed to the Ni $2p_{3/2}$ spin–orbit levels of NiO.[11,38] A weak peak is found at 852.4 eV, which can be ascribed to Ni^0.[39] So there are two kinds of nickel atoms in A-2-650 NiO_x–C fibers, including NiO and Ni^0 with a molar ratio of 6.1 to 93.9, which agree with the results of TEM. The fine XPS spectrum of O 1s is displayed in Fig. 5c, which can be deconvoluted to five peaks using a Gaussian fit. The peak at 529.7 eV is of low intensity, and it can be probably

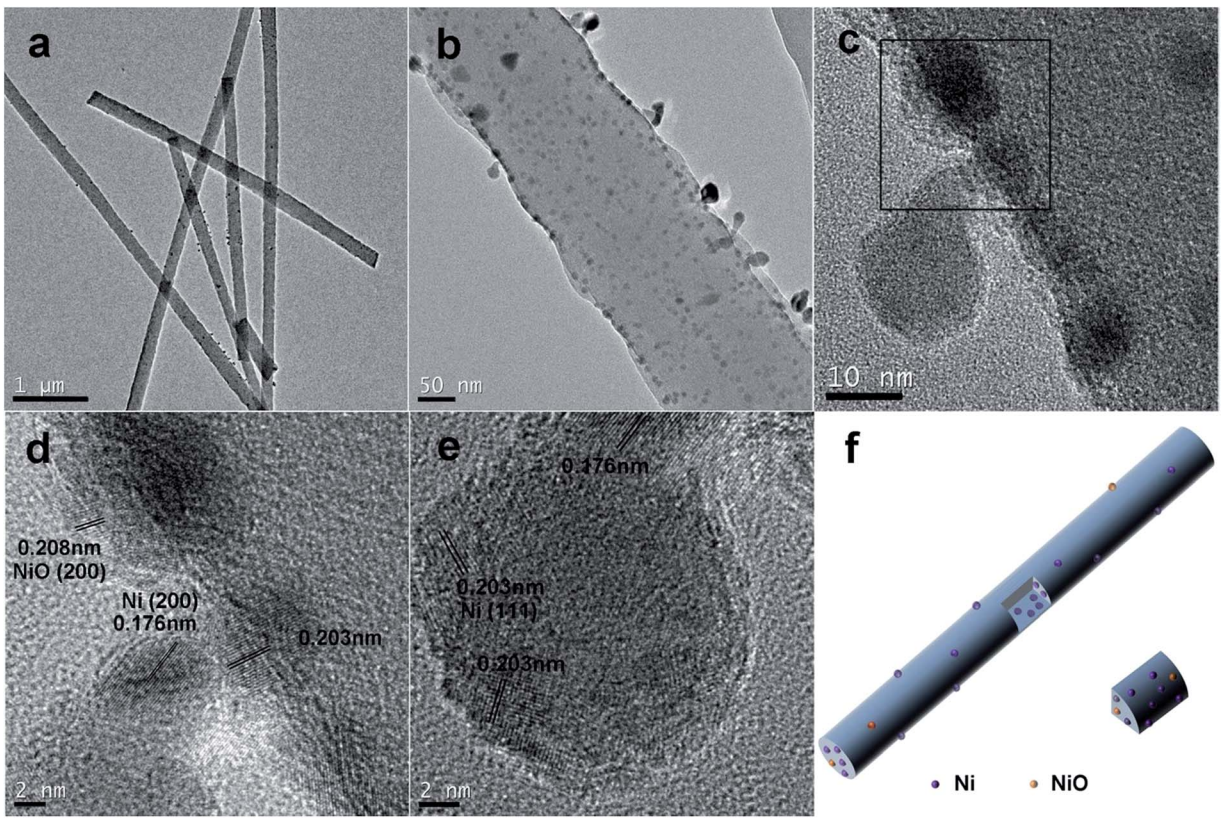

Fig. 4 TEM images of NiO_x–C fibers (A-2-650) at different magnifications. (d) Shows the amplified image of the marked field in (c). (e) Displays a high-resolution image of the nanoparticle in (c). (f) Displays a scheme to show that the nanoparticles outside the nanowire almost are Ni^0.

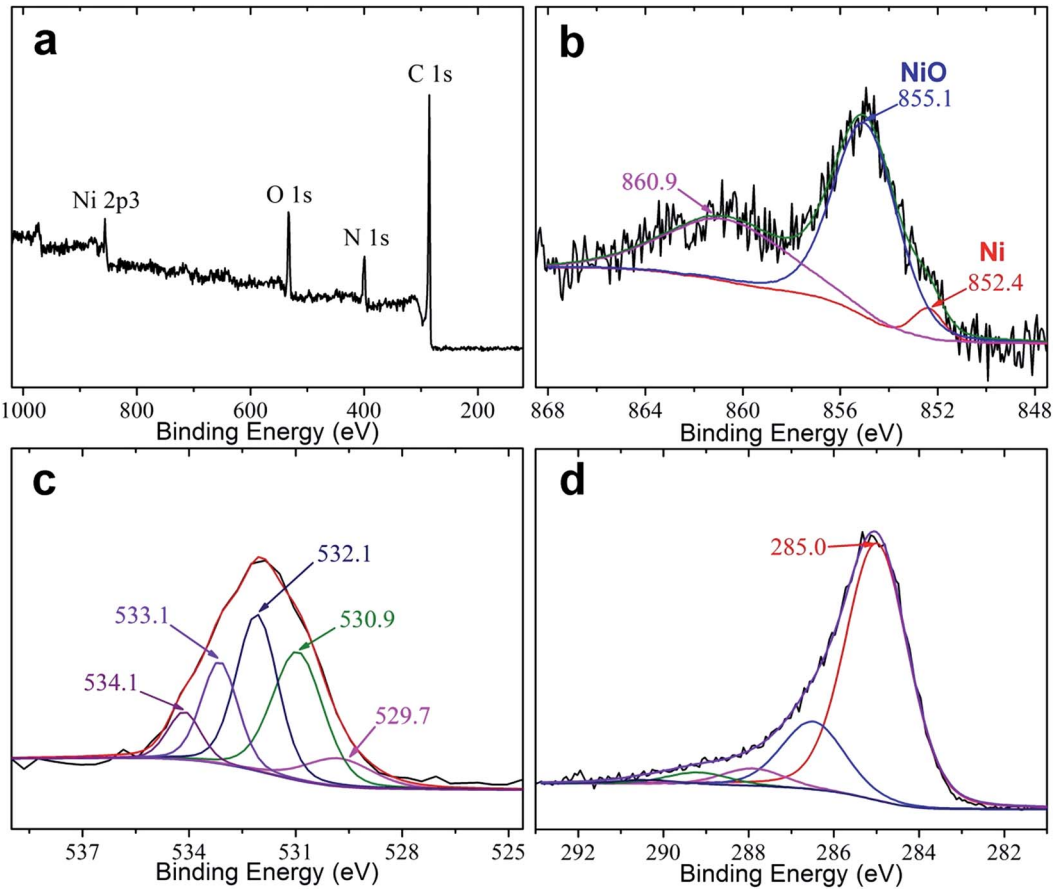

Fig. 5 (a) XPS spectrum of A-2-650 NiO_x–C fibers; (b–d) show the fine XPS spectra of Ni 2p (b), O 1s (c) and C 1s (d).

due to the O 1s in NiO.[4,11] The relative low intensity may be ascribed to the encapsulation of NiO in carbon fibers. The peaks at 532.1, 533.1, and 534.1 eV correspond to C═O, C–OH (and/or C–O–C), and chemical sorbed oxygen (and perhaps adsorbed waters).[40,41] The extra peak at 530.9 eV may be attributed to the possible present of Ni–O–C binds because Ni–C bonds are approximately located at either 853 or 285 eV.[11] The XPS spectrum of C 1s shown in Fig. 5d can be deconvoluted to five peaks at 290.4, 289.2, 287.9, 286.5, and 285 eV. Those data are consistent with our previous results about PAN-based carbon fibers.[23] Thus NiO_x nanoparticles, including NiO and Ni^0, are anchored on carbon fibers by chemical bonds other than mechanical force and Van der Waals' force.

Fig. 6 shows the cyclic voltammetry (CV) curves of pure carbon fibers (E650) and A-2-650 NiO_x–C fibers. As shown in Fig. 6a, the CV curve of E650 in the first cycle exhibits a clear cathodic peak at approximately 0.3 V, resulting from the irreversible formation of SEI films.[28] It shows two anodic peaks at about 0.2 and 1.3 V, corresponding to the delithiation of graphite-like carbon and lithium extraction from the defective sites (and/or micropores) of carbon fibers.[42–44] The CV curve in the second cycle nearly overlaps with the fourth one, indicating a good cyclic stability of E650. The initial lithiation potential of NiO_x–C fibers is approximate 0.5 V, similar to that of a previous report about nickel–carbon fibers.[27] A board anodic peak in the

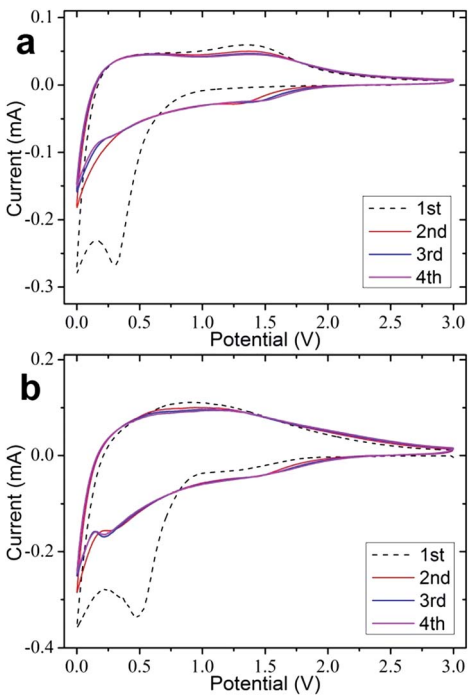

Fig. 6 CV curves of pure carbon fibers E650 (a) and NiO_x–C fibers A-2-650 (b) at a scan rate of 0.3 mV s^{-1} in a range of 0–3 V.

range of 0.5 to 1.3 V is found in the first delithiation procedure, which is almost unchanged in the subsequent cycles. The typical cathodic and anodic peaks of NiO are located at approximately 1.1 and 2.2 V.[10,45,46] Therefore, the board anodic peak cannot be indexed to the delithiation of Ni^0 and Li_2O. In some of reports about NiO or NiO-based composites as anode for LIBs, the anodic peak at about 1 V was attributed to the partial decomposition of SEI films.[14–16,28] Whereas, the anodic peak at about 1 V only is observed in the first cycle in those studies. In present investigation, the result is different from above papers that the peak potential and relative intensities of the anodic peak in the second and fourth cycle are almost the same. So, the board peak may not arise from the partial decomposition of SEI films. According to the mechanism that lithium ions could be stored in micropores and defective sites of carbon with high capacities, the board peak of A-2-650 at 1 V is attributed to the storage of lithium ions in micropores and disordered carbon. In addition, the present of NiO_x results in the shift of this peak to a lower potential, showing the activation effect of NiO_x.

Fig. 7a shows the voltage profile of A-2-650 NiO_x–C fibers in the 1st, 2nd, 15th, and 200th cycle. In the 1st cycle, A-2-650 NiO_x–C fibers delivers a discharge capacity of 1203 mA h g^{-1} at a current density of 100 mA g^{-1}, corresponding to a Coulombic efficiency of 80%. During the discharge procedure, an extended voltage plateau is found around 1 V, which may be attributed to the formation of SEI films.[11,28] A more inclined discharge slope in the range of 0.8 to 0.005 V is observed, which could be ascribed to the partial capacity contribution from carbon fibers.[28] In the subsequent discharge process, the plateau becomes higher and more sloping than those in the 1st cycle, showing that the lithiation reaction becomes easier. When the current density increases to 500 mA g^{-1}, the charge curve in the 15th cycle almost overlaps with that in the 200th cycle, indicating the excellent cyclic properties of A-2-650 NiO_x–C fibers.

Fig. 7b compares the specific capacities of NiO_x–C fibers obtained at different temperatures, and corresponding Coulombic efficiencies are shown in Fig. 7c. The current density in the first ten cycles is 100 mA g^{-1}, which increases to 500 mA g^{-1} in the subsequent cycles. NiO_x–C fibers synthesized at 550 °C (A-2-550) could deliver specific capacities of 487 and 345 mA h g^{-1} in the 10th and 200th cycles. As the annealing temperature increasing to 600 °C, the corresponding capacities of NiO_x–C fibers (A-2-600) enhance to 578 and 387 mA h g^{-1}, showing positive effects of improving annealing temperature on the electrochemical properties of NiO_x–C fibers.[47] The capacity increase of both A-2-550 and A-2-600 can be ascribed to the activation of NiO_x and the electrolyte solvent soakage into composites.[22,36,48] When the annealing temperature was set at 650 °C, the resulting NiO_x–C fibers (A-2-650) could store lithium

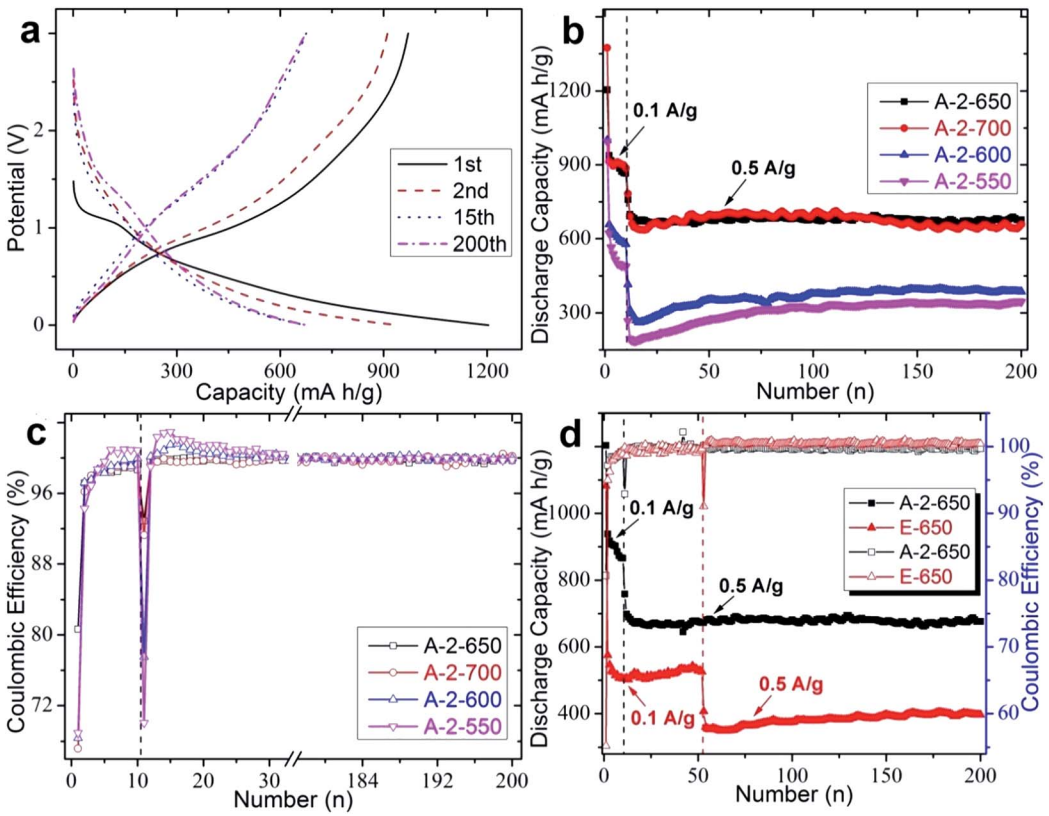

Fig. 7 (a) Displays the charge–discharge profiles of A-2-650 NiO_x–C fibers in different cycles at 100 mA g^{-1}; (b) and (c) show the specific capacities, cyclic stability, and Coulombic efficiencies of NiO_x–C fibers obtained at different temperatures. (d) Compares the electrochemical properties of A-2-650 NiO_x–C fibers and E650 pure carbon fibers at current densities of 100 and 500 mA g^{-1}. All of the specific capacities in this study were calculated based on the weight of the total networks.

ions with capacities of 865 and 676 mA h g^{-1} in the 10th and 200th cycles. The samples (A-2-700) prepared at 700 °C can deliver capacities of 887 and 658 mA h g^{-1} in corresponding cycles, whose properties are very close to those of A-2-650. In addition, the ratio of the specific capacities in the 200th cycle to that in the 10th cycle are 0.71, 0.67, 0.78, and 0.74 along with the increase of annealing temperature from 550 to 700 °C, indicating A-2-650 with the highest retention ratio. Besides, the Coulombic efficiencies of A-2-650 almost maintain at 99.5% in all the cycles except the 1st and 11th cycles, showing an excellent cyclic stability. Because a high annealing temperature can result in carbon fibers with high graphitization degree and conductivity and may cause the transformation of NiO to Li-inactive Ni^0, the A-2-650 NiO_x–C fibers with best properties may be attributed to the annealing temperature of 650 °C which can make a balance between the high electrical conductivity of carbon fibers and avoiding the conversion of NiO to Ni^0 and the reduction of nitrogen concentration in carbon fibers.[18,22]

The electrochemical properties of A-2-650 NiO_x–C fibers and E650 pure carbon fibers are compared in Fig. 7d. They display nearly unchanged Coulombic efficiencies and specific capacities at constant current densities, indicating good cyclic stability of carbon fibers-based composites. Whereas, A-2-650 could deliver a specific capacity of 865 mA h g^{-1} at a current density of 100 mA g^{-1}, which is 1.7 times that of E650. In addition, the specific capacity of A-2-650 at 500 mA g^{-1} is 676 mA h g^{-1}, also 280 mA h g^{-1} higher than that of E650 at the corresponding cycle. Therefore, the NiO_x nanoparticles even with very low concentration have great effects on improving the properties of carbon fibers regards the storage of lithium ions. The improvement may be ascribed to the micropores and/or defect sites arising from the present of NiO_x because the possible present of Ni–O–C chemical bonds according to XPS results.

NiO_x–C fibers were further characterized by rate capacity tests, and the results are shown in Fig. 8a. It can be found that A-2-650 maintains reversible capacities of 687, 601, 500, 423, and 319 mA h g^{-1} at current densities of 0.1, 0.2, 0.5, 1, and 2 A g^{-1}, respectively. After the current density decreases to 0.1 A g^{-1}, their capacities quickly increase to 790 mA h g^{-1}. The improved capacity as compare to the original value can be attributed to the activation of the embedded NiO in carbon fiber matrix and electrolyte solvent soakage, and similar phenomena have been found in previous reports about electrospun composites for LIBs.[22,36,48] Comparing the rate capacities of A-2-650 (with 9.2 wt% NiO_x), C-2-650 (with 17.1 wt% NiO_x), and E650 (pure carbon fibers), it can be concluded that the concentration of NiO_x in carbon fibers should be controlled at approximate 9.2 wt% because the rare property of A-2-650 is the best one among those three samples. The property of A-2-650 is also better than that of A-2-600. A possible reason is that the relative higher temperature would result in carbon fiber with high conductivity which is of benefit for the electron transfer and the reduction of polarization.[22,47]

AC impedance experiments were carried out after rate capacity tests to investigate the reason why A-2-650 NiO_x–C fibers were of excellent properties. The Nyquist plots of these

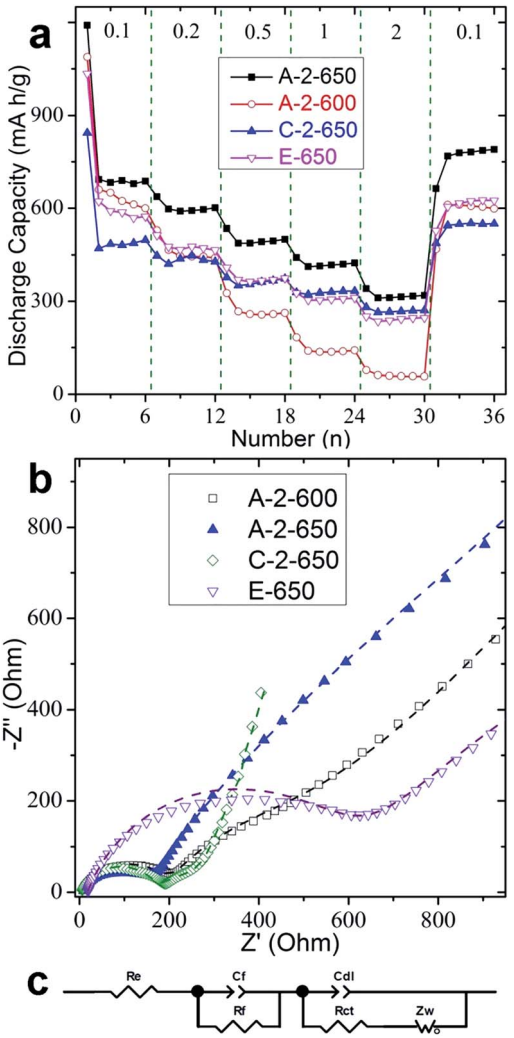

Fig. 8 (a) Displays specific capacities of NiO_x–C fibers (A-2-650, A-2-600, and C-2-650) and pure carbon fibers (E650) at various current densities (A g^{-1}). (b) Shows the Nyquist plots of NiO_x–C fibers and pure carbon fibers after the rate capacity tests. The dash lines are the corresponding fitting results. (c) Is the equivalent circuit used for fitting experimental data.

samples in Fig. 8b are composed of two partially overlapped semicircles at high- and medium-frequency ranges, and an inclined line in the low frequency range which could be considered as Warburg impedance.[49–51] The AC impedance results were fitted using an equivalent circuit, as shown in Fig. 8c. The intercepts of four curves on the Z real axis are almost the same values, suggesting the uniform electrolyte resistance (R_e). C_f and R_f are the capacitance and resistance of the SEI films (high-frequency). C_{dl} and R_{ct} are the double-layer capacitance and charge-transfer resistance (medium-frequency). According to the equivalent circuit, the fitting values of R_f are 161, 170, and 576 Ω for A-2-600, C-2-650, and E-650 while it is 136 Ω for A-2-650, showing a lowest R_f of A-2-650. The R_{ct} of A-2-600,A-2-650, and C-2-650 are 394, 178, and 161 Ω which are lower than that of E650, indicating that nickel may enhance the graphitization of carbon resulting in an

improved conductivity.[9] Besides, it can be found by comparing the R_{ct} of A-2-650 with A-2-600 that an improved heat treatment temperature results in an increased graphitization and conductivity of carbon. Although the R_{ct} of C-2-650 is lower than that of A-2-650, the sum of R_{ct} and R_f is 314 Ω for A-2-650 which is lower than that of C-2-650 (331 Ω). Considering the differences of heat treatment temperatures, and NiO_x concentrations and distribution in those NiO_x–C fibers, the excellent properties of A-2-650 could be ascribed to their high conductivity arising from improved graphitization carbon fibers and the possible Ni–O–C bonds. In addition, the network composed of NiO_x–C fibers improves the contact area between the active materials and electrolyte, shorten the transfer distance of lithium ions, and are favor for the fast diffusion of lithium ions.[23,48]

4 Conclusions

NiO_x–C fibers with controllable content of NiO_x can be synthesized *via* a simple electrospinning approach and following thermal treatment. NiO_x is demonstrated to be complex including both NiO and Ni^0 other than a single component. NiO_x–C fibers obtained at 650 °C with the homogenous distribution of 9.2 wt% NiO_x nanoparticles could deliver a reversible capacity of 865 and 676 mA h g^{-1} at a current density of 100 and 500 mA g^{-1} in the 11^{th} and 200^{th} cycles, respectively. Those properties are better than those of both pure carbon fibers and NiO_x–C fibers with different either NiO_x concentrations or annealing temperatures. Besides, the rate capacities of NiO_x–C fibers synthesized at 650 °C with 9.2 wt% NiO_x are also better than other anodes. The enhanced properties of NiO_x–C fibers could be ascribed to the micropores and/or defective sites arising from the present of NiO_x nanoparticles, and the network of carbon fibers to accelerate the transfer of electrons and the diffusion of lithium ions. It is believed that this study may provide a new insight to synthesize carbon-transition metal (oxide) with high properties for energy storage.

Acknowledgements

This research work has been financially supported in part by the National Natural Science Foundation of China (51404103, 61376073 and 21103046), the Hunan Provincial Natural Science Foundation of China (11JJ7004, 14JJ3067), and Fundamental Research Funds for the Central Universities.

Notes and references

1 M. Naguib, J. Halim, J. Lu, K. M. Cook, L. Hultman, Y. Gogotsi and M. W. Barsoum, *J. Am. Chem. Soc.*, 2013, **135**, 15966–15969.
2 Y. Wang, Y. Wang, D. Jia, Z. Peng, Y. Xia and G. Zheng, *Nano Lett.*, 2014, **14**, 1080–1084.
3 M.-K. Song, S. Park, F. M. Alamgir, J. Cho and M. Liu, *Mater. Sci. Eng., R*, 2011, **72**, 203–252.
4 L. Liu, Y. Li, S. Yuan, M. Ge, M. Ren, C. Sun and Z. Zhou, *J. Phys. Chem. C*, 2009, **114**, 251–255.
5 D.-H. Lee, J.-C. Kim, H.-W. Shim and D.-W. Kim, *ACS Appl. Mater. Interfaces*, 2014, **6**, 137–142.
6 R. Sahay, P. Suresh Kumar, V. Aravindan, J. Sundaramurthy, W. Chui Ling, S. G. Mhaisalkar, S. Ramakrishna and S. Madhavi, *J. Phys. Chem. C*, 2012, **116**, 18087–18092.
7 M. Zhang, D. Lei, X. Yin, L. Chen, Q. Li, Y. Wang and T. Wang, *J. Mater. Chem.*, 2010, **20**, 5538–5543.
8 P.-L. Taberna, S. Mitra, P. Poizot, P. Simon and J.-M. Tarascon, *Nat. Mater.*, 2006, **5**, 567–573.
9 Y. Chen, X. Li, X. Zhou, H. Yao, H. Huang, Y.-W. Mai and L. Zhou, *Energy Environ. Sci.*, 2014, **7**, 2689–2696.
10 V. Aravindan, P. Suresh Kumar, J. Sundaramurthy, W. C. Ling, S. Ramakrishna and S. Madhavi, *J. Power Sources*, 2013, **227**, 284–290.
11 G. Zhou, D.-W. Wang, L.-C. Yin, N. Li, F. Li and H.-M. Cheng, *ACS Nano*, 2012, **6**, 3214–3223.
12 Y. Huang, X.-l. Huang, J.-s. Lian, D. Xu, L.-m. Wang and X.-b. Zhang, *J. Mater. Chem.*, 2012, **22**, 2844–2847.
13 G. Zhang, L. Yu, H. E. Hoster and X. W. Lou, *Nanoscale*, 2013, **5**, 877–881.
14 M. M. Rahman, S.-L. Chou, C. Zhong, J.-Z. Wang, D. Wexler and H.-K. Liu, *Solid State Ionics*, 2010, **180**, 1646–1651.
15 Y. Xia, W. Zhang, Z. Xiao, H. Huang, H. Zeng, X. Chen, F. Chen, Y. Gan and X. Tao, *J. Mater. Chem.*, 2012, **22**, 9209–9215.
16 X. H. Huang, J. P. Tu, C. Q. Zhang, X. T. Chen, Y. F. Yuan and H. M. Wu, *Electrochim. Acta*, 2007, **52**, 4177–4181.
17 X. H. Huang, J. P. Tu, C. Q. Zhang and J. Y. Xiang, *Electrochem. Commun.*, 2007, **9**, 1180–1184.
18 C. Xu, J. Sun and L. Gao, *J. Power Sources*, 2011, **196**, 5138–5142.
19 Y. J. Mai, S. J. Shi, D. Zhang, Y. Lu, C. D. Gu and J. P. Tu, *J. Power Sources*, 2012, **204**, 155–161.
20 M. Zhang, D. Lei, Z. Du, X. Yin, L. Chen, Q. Li, Y. Wang and T. Wang, *J. Mater. Chem.*, 2011, **21**, 1673–1676.
21 G. Ji, B. Ding, Z. Sha, J. Wu, Y. Ma and J. Y. Lee, *Nanoscale*, 2013, **5**, 5965–5972.
22 L. Wang, Y. Yu, P. C. Chen, D. W. Zhang and C. H. Chen, *J. Power Sources*, 2008, **183**, 717–723.
23 M. Zhang, E. Uchaker, S. Hu, Q. Zhang, T. Wang, G. Cao and J. Li, *Nanoscale*, 2013, **5**, 12342–12349.
24 M. Zhang, F. Yan, X. Tang, Q. Li, T. Wang and G. Cao, *J. Mater. Chem. A*, 2014, **2**, 5890–5897.
25 J. Zhu, D. Lei, G. Zhang, Q. Li, B. Lu and T. Wang, *Nanoscale*, 2013, **5**, 5499–5505.
26 J. Lee, C. Jo, B. Park, W. Hwang, H. I. Lee, S. Yoon and J. Lee, *Nanoscale*, 2014, **6**, 10147–10155.
27 B. Wang, J. Cheng, Y. Wu, D. Wang and D. He, *J. Mater. Chem. A*, 2013, **1**, 1368–1373.
28 L. Ji, Z. Lin, M. Alcoutlabi, O. Toprakci, Y. Yao, G. Xu, S. Li and X. Zhang, *RSC Adv.*, 2012, **2**, 192–198.
29 L. Ji, Z. Lin, A. J. Medford and X. Zhang, *Chem.–Eur. J.*, 2009, **15**, 10718–10722.
30 J. H. Pan, Q. Huang, Z. Y. Koh, D. Neo, X. Z. Wang and Q. Wang, *ACS Appl. Mater. Interfaces*, 2013, **5**, 6292–6299.
31 Y. Ni, Y. Yin, P. Wu, H. Zhang and C. Cai, *ACS Appl. Mater. Interfaces*, 2014, **6**, 7346–7355.

32 S.-X. Wang, L. Yang, L. P. Stubbs, X. Li and C. He, *ACS Appl. Mater. Interfaces*, 2013, **5**, 12275–12282.
33 J. Li, E.-h. Liu, W. Li, X.-y. Meng and S.-t. Tan, *J. Alloys Compd.*, 2009, **478**, 371–374.
34 K. Otsuka, Y. Abe, N. Kanai, Y. Kobayashi, S. Takenaka and E. Tanabe, *Carbon*, 2004, **42**, 727–736.
35 R. Brown, M. E. Cooper and D. A. Whan, *Appl. Catal.*, 1982, **3**, 177–186.
36 L. Wang, Y. Yu, P.-C. Chen and C.-H. Chen, *Scr. Mater.*, 2008, **58**, 405–408.
37 P. Poizot, S. Laruelle, S. Grugeon, L. Dupont and J. M. Tarascon, *Nature*, 2000, **407**, 496–499.
38 B. Varghese, M. V. Reddy, Z. Yanwu, C. S. Lit, T. C. Hoong, G. V. Subba Rao, B. V. R. Chowdari, A. T. S. Wee, C. T. Lim and C.-H. Sow, *Chem. Mater.*, 2008, **20**, 3360–3367.
39 A. P. Grosvenor, M. C. Biesinger, R. S. C. Smart and N. S. McIntyre, *Surf. Sci.*, 2006, **600**, 1771–1779.
40 S. D. Gardner, C. S. K. Singamsetty, G. L. Booth, G.-R. He and C. U. Pittman Jr, *Carbon*, 1995, **33**, 587–595.
41 Y. Xie and P. M. A. Sherwood, *Chem. Mater.*, 1990, **2**, 293–299.
42 N. Takami, A. Satoh, M. Oguchi, H. Sasaki and T. Ohsaki, *J. Power Sources*, 1997, **68**, 283–286.
43 Y.-P. Wu, C.-R. Wan, C.-Y. Jiang, S.-B. Fang and Y.-Y. Jiang, *Carbon*, 1999, **37**, 1901–1908.
44 B. Guo, X. Wang, P. F. Fulvio, M. Chi, S. M. Mahurin, X.-G. Sun and S. Dai, *Adv. Mater.*, 2011, **23**, 4661–4666.
45 X. Li, A. Dhanabalan and C. Wang, *J. Power Sources*, 2011, **196**, 9625–9630.
46 X. H. Huang, J. P. Tu, B. Zhang, C. Q. Zhang, Y. Li, Y. F. Yuan and H. M. Wu, *J. Power Sources*, 2006, **161**, 541–544.
47 J. K. Lee, K. W. An, J. B. Ju, B. W. Cho, W. I. Cho, D. Park and K. S. Yun, *Carbon*, 2001, **39**, 1299–1305.
48 W.-H. Ryu, J. Shin, J.-W. Jung and I.-D. Kim, *J. Mater. Chem. A*, 2013, **1**, 3239–3243.
49 M. Umeda, K. Dokko, Y. Fujita, M. Mohamedi, I. Uchida and J. Selman, *Electrochim. Acta*, 2001, **47**, 885–890.
50 S. Yang, X. Feng, S. Ivanovici and K. Müllen, *Angew. Chem., Int. Ed.*, 2010, **49**, 8408–8411.
51 M. Zhang, B. Qu, D. Lei, Y. Chen, X. Yu, L. Chen, Q. Li, Y. Wang and T. Wang, *J. Mater. Chem.*, 2012, **22**, 3868–3874.